



HAL
open science

Earthquake focal mechanisms and stress inversion in the Irpinia Region (southern Italy)

Giuseppe Pasquale, Raffaella Matteis, Annalisa Romeo, Rosalba Maresca

► **To cite this version:**

Giuseppe Pasquale, Raffaella Matteis, Annalisa Romeo, Rosalba Maresca. Earthquake focal mechanisms and stress inversion in the Irpinia Region (southern Italy). *Journal of Seismology*, 2008, 13 (1), pp.107-124. 10.1007/s10950-008-9119-x . hal-00478435

HAL Id: hal-00478435

<https://hal.science/hal-00478435>

Submitted on 30 Apr 2010

HAL is a multi-disciplinary open access archive for the deposit and dissemination of scientific research documents, whether they are published or not. The documents may come from teaching and research institutions in France or abroad, or from public or private research centers.

L'archive ouverte pluridisciplinaire **HAL**, est destinée au dépôt et à la diffusion de documents scientifiques de niveau recherche, publiés ou non, émanant des établissements d'enseignement et de recherche français ou étrangers, des laboratoires publics ou privés.

Earthquake focal mechanisms and stress inversion in the Irpinia Region (southern Italy)

Giuseppe Pasquale · Raffaella De Matteis ·
Annalisa Romeo · Rosalba Maresca

Received: 29 February 2008 / Accepted: 30 June 2008 / Published online: 17 August 2008
© Springer Science + Business Media B.V. 2008

Abstract The goal of this study was to estimate the stress field acting in the Irpinia Region, an area of southern Italy that has been struck in the past by destructive earthquakes and that is now characterized by low to moderate seismicity. The dataset are records of 2,352 aftershocks following the last strong event: the 23 November 1980 earthquake (M 6.9). The earthquakes were recorded at seven seismic stations, on average, and have been located using a three-dimensional (3D) P-wave velocity model and a probabilistic, non-linear, global search technique. The use of a 3D velocity model yielded a more stable estimation of take-off angles, a crucial parameter for focal mechanism computation. The earthquake focal mechanisms were computed from the P-wave first-motion polarity data using the FPFIT algorithm. Fault plane solutions show mostly normal component faulting (pure normal fault and normal fault with a strike-slip component). Only some fault plane solutions show strike-slip and reverse faulting. The stress field is estimated using the method proposed by

Michael (J Geophys Res 92:357–368, 1987a) by inverting selected focal mechanisms, and the results show that the Irpinia Region is subjected to a NE–SW extension with horizontal σ_3 (plunge 0° , trend 230°) and subvertical σ_1 (plunge 80° , trend 320°), in agreement with the results derived from other stress indicators.

Keywords Irpinia Region · Seismicity · Focal mechanisms · Stress inversion

1 Introduction

The state of stress within the Earth's crust is of particular interest for geologists and geophysicists as it can provide a better understanding of geodynamic processes (Bott 1959; McKenzie 1969). The most common methods to determine principal stress orientations are that using breakout data from borehole measurements, which can only be performed at near surface depths (McGarr and Gay 1978), and that using slickenside data. However, in most cases, earthquakes do not show surface ruptures. For this reason, the background seismicity and the aftershocks of a strong earthquake represent the only tools to study the state of stress acting in a region at great depth. Consequently, the use of focal mechanisms to estimate the nature of the stress tensor in the seismogenic zone has been frequently used in the past

G. Pasquale (✉) · R. De Matteis · R. Maresca
Dipartimento di Studi Geologici ed Ambientali,
Università degli Studi del Sannio, Benevento, Italy
e-mail: gpasqual@unisannio.it

A. Romeo
AMRA Scarl, Napoli, Italy

(i.e., Gephart and Forsyth 1984; Rivera and Cisternas 1990; Michael 1984; Angelier 1990).

In this study, we have analyzed the seismicity in the Irpinia Region to determine the stress field. It belongs to the most active seismic zones of the Southern Apennines characterized by large destructive earthquakes that occurred both in historical and recent times; the last and strongest of these events was the 23 November 1980 earthquake (M 6.9). This earthquake is the best documented Italian seismic event (Giardini 1993; Del Pezzo et al. 1983; Deschamps and King 1984; Westaway and Jackson 1987; Bernard and Zollo 1989; Pantosti and Valensise 1990), and was structured into three main rupture episodes (known as those of 0 s, 20 s, and 40 s) that were associated with a surface rupture of about 40 km (Amato et al. 1992). The focal mechanism of this event showed a dominant normal faulting.

The stress field in this region, determined using moderate to strong earthquake focal mechanisms and fault and breakout data, reveals that the Southern Apennines is generally ongoing through a NE–SW extension.

The aim of the present study was to obtain information about the stress field using low magnitude earthquakes. In particular, we used aftershocks of the 23 November 1980 earthquake (M 6.9) to determine the best homogeneous stress tensor, and to compare it with results obtained by other methodologies.

The principal stress orientations can be determined directly from earthquake focal mechanisms through the use of inversion techniques. These techniques yield four parameters: three unit vectors which specify the maximum, minimum, and intermediate compressive principal stress axis orientations and a scalar which describes the relative magnitudes of the principal stresses (Gephart and Forsyth 1984; Michael 1984; Angelier 1990). The accuracy of these inversion techniques depends on the uncertainty of the focal mechanisms and the fault/auxiliary plane ambiguity. In addition to these methods, Rivera and Cisternas (1990) developed a method whose major advance is to use not previously determined focal mechanisms but the original data that is the polarities of the P arrival and take-off angles for source-station pairs. The focal mechanisms are a by-product of the inverse

problem. This method could be useful when the number of the polarities is scarce to determine reliable focal mechanisms.

In this study, we have computed the focal mechanisms of earthquakes located in 3D and 1D velocity models in order to estimate the improvement due to the knowledge of a more realistic model.

We have used the technique developed by Michael (1987a) for inverting focal mechanisms. This technique defines the confidence regions on the quantities obtained through a statistical tool that is known as bootstrap resampling.

2 Geological and structural setting

Intense hydrocarbon exploration in the Southern Apennines has provided numerous seismic reflection and well data, which have favored the definition of structural models of the Southern Apennines and the reconstruction of its tectonic evolution.

The Apennines are the result of a complex sequence of tectonic events that were associated with the collision between the African and European plate (McKenzie 1972). They are located between the rather aseismic Tyrrhenian Sea to the West and the compressional Adriatic Sea–Dinarides domain to the East. Over a distance of 100 km or less, there is the change from the active extensional domain of the inner Apennines to areas of active folding and thrusting in the Adriatic Sea (Pantosti and Valensise 1990).

The compressional tectonics started in the Middle Cretaceous period and lasted until the Oligocene with the continental collision. In the Tortonian age, the rift process started and caused the opening of the Tyrrhenian Basin. Then, following the hinge roll-back of the subducting Adriatic plate, the compressional tectonics migrated towards the East (Patacca and Scandone 1989; Patacca et al. 1990).

The Southern Apennines is a duplex system (Patacca et al. 1990) transported over the flexured southwestern margin of the Apulia foreland. This duplex system consists of a complex architecture of carbonate horsts deriving from the Apulia Carbonate Platform, which is overthrust

by rootless nappes. The belt is associated with the Tyrrhenian back-arc basin to the West and with the Bradano foredeep to the East. From Late Tortonian to Lower-Middle Pleistocene, the basin–thrust-belt–foredeep system migrated eastwards, and progressively involved both the basin and carbonate platform paleogeographic domains (D’Argenio et al. 1974) (Fig. 1). Investigations into the Southern Apennines have highlighted the extreme structural complexity of the thrust belt that is due to several factors. The tectonic style is variable since the basin facies terrains were mainly subjected to ductile deformation, whereas the carbonate platform sequences underwent brittle deformation (Menardi and Rea 2000). More-

over, the kinematic evolution was characterized by out-of-sequence, thrust-propagation processes (Roure et al. 1991). In addition, the belt was split up into segments, which underwent different tectonic evolution. In particular, the mountain chain can be subdivided into two major arcs: the NNW–SSE-trending, Molise–Sannio arc to the north, and the WNW–ESE-trending, Campania–Lucania arc to the south, which join in the Irpinia Region.

Finally, starting from the Early-Middle Pleistocene, the axial zone of the chain underwent NE–SW extensional tectonics. This change in the tectonic regime was the cause of extensive volcanism on the Tyrrhenian margin of the chain and the

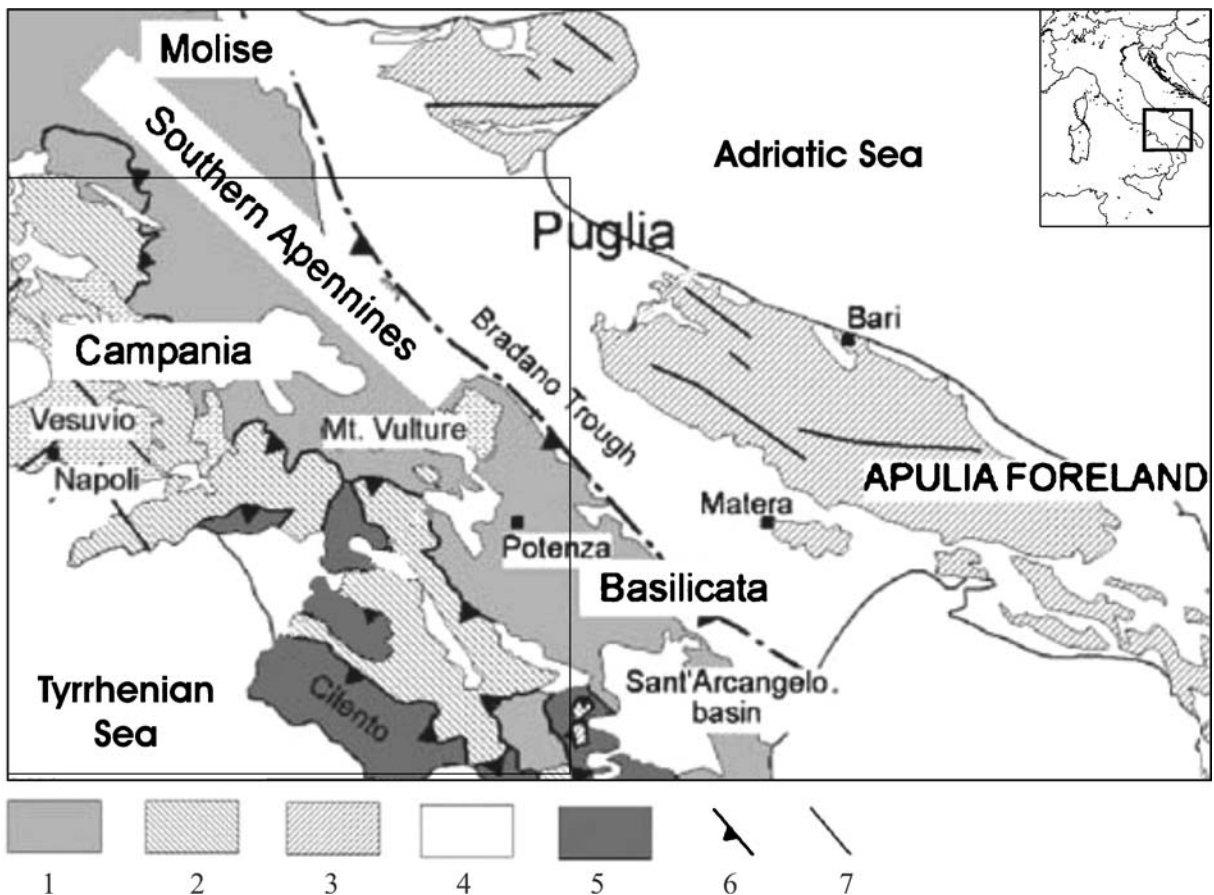


Fig. 1 Simplified geological map of the Southern Apennines showing the major structural features (modified from Tiberti et al. 2005). 1 Molise–Sannio–Lagonegro pelagic basin and related foredeep deposits; 2 Apennine

carbonate platform; 3 Apulia carbonate platform; 4 Pliocene–Quaternary terrigenous deposits; 5 Ligurides and Sicilides; 6 main thrust fronts; 7 main faults. The box represents the location of Fig. 2

development of large extensional and transtensional structures, which crosscut the pre-existing compressional structures, thus further complicating the internal geometry of the thrust belt. This extensional stress regime causes the seismicity of the Southern Apennines, with large earthquakes centered on the axis of the belt, with depths of mainly around 20 km and characterized by normal faulting focal mechanisms.

3 Earthquake locations

In this work, we analyzed the earthquakes ($M < 4$) that occurred immediately after the 23 November 1980 main shock (M 6.9). These were recorded by the National Institute of Geophysics and Volcanology (*Istituto Nazionale di Geofisica e Vulcanologia*; INGV) seismic network and by a temporary mobile seismic network which was installed in the epicentral area a few days after the mainshock (Fig. 2).

The dataset consists of 2,352 earthquakes recorded by seven stations, on average, resulting in a total of about 21,000 P-wave and 6,700 S-wave arrival time picks and 7,620 P-wave polarity recordings. The location of the earthquakes needs *a priori* the knowledge of the crustal velocity model. Various one-dimensional (1D) velocity models have been determined in different studies: Deschamps and King (1984), Bernard and Zollo (1989), and Amato et al. (1992) used aftershock arrival times of the 1980 earthquakes to constrain velocities; Improta et al. (2000) determined the velocity structure by interpretation and integration of gravity data, seismic reflection lines, deep wells, and subsurface constraints for the Irpinia Region, up to 7 km in depth. We located the earthquakes using the different 1D velocity models available in literature. The 1D velocity model that minimizes the residuals between the theoretical and observed first P-wave and S-wave travel times is that proposed by Bernard and Zollo (1989).

More recently, Romeo et al. (2007) computed a 3D P-wave crustal velocity model in the epicentral area of the 1980 Irpinia earthquake using travel times of aftershocks and background seismicity that occurred from 1988 to 2004 in the Irpinia Region. The volume investigated was 144×162

$\times 30 \text{ km}^3$, and it was discretized with cell sizes of $9 \times 9 \times 3 \text{ km}^3$, with the best resolved zone extending from 0 km to about 20 km in depth. This model overlaps with the volume of the present study.

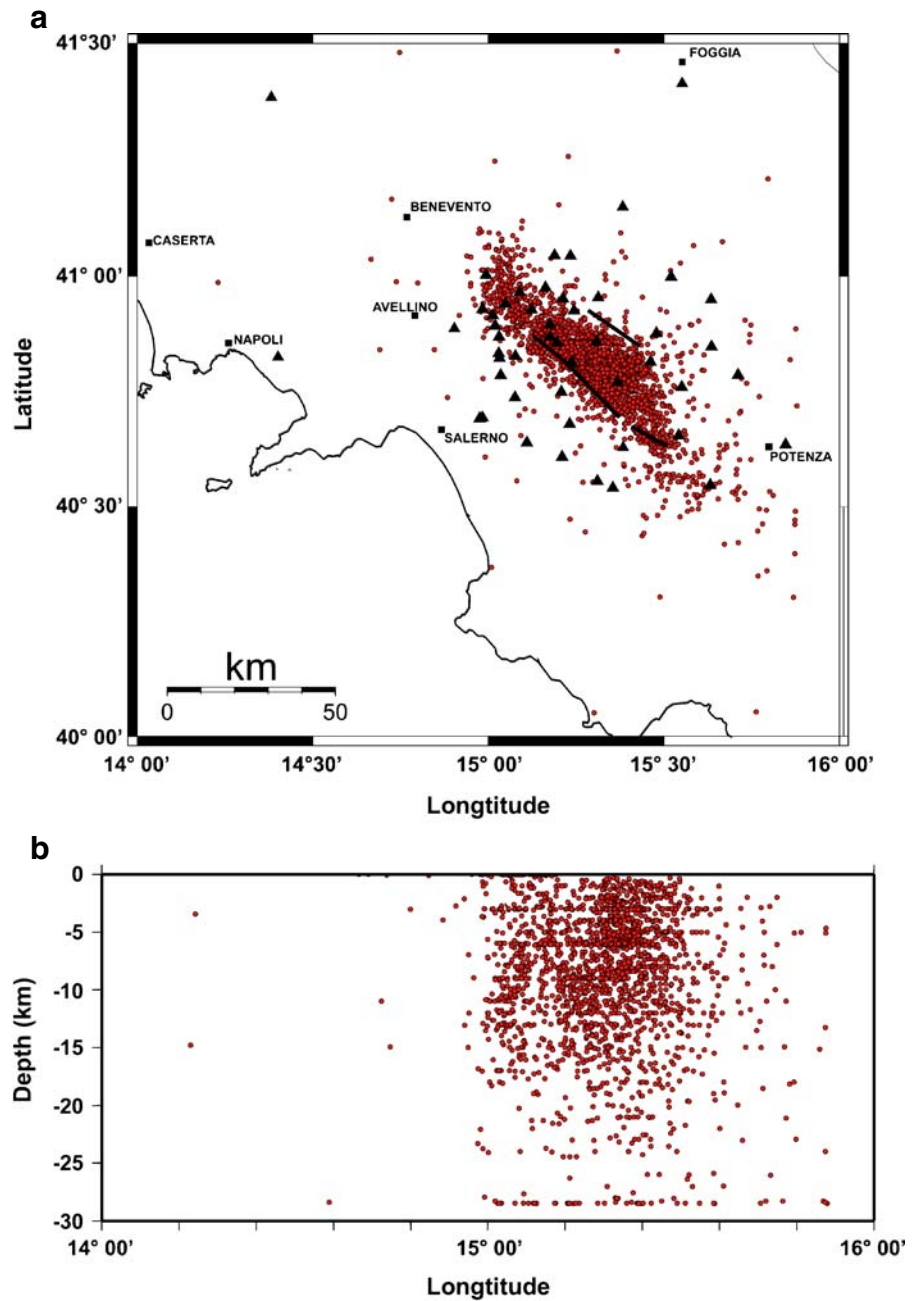
Considering that: (1) the top of the crustal velocity model corresponds to sea level; and (2) in the area, some stations are located over 1,000 m a.s.l., the present study needed to take into account station corrections. For each station, we identified the outcropping stratigraphic–structural units using geological maps (Amanti et al. 2002). Then we associated a correction velocity to each station taking into account the results of Improta et al. (2000, 2003). Finally, on the ground of a vertical ray path, we computed station delays.

The hypocenter parameters were computed again using the Romeo et al. (2007) 3D velocity model with the probabilistic, non-linear, global search earthquake location method (NonLinLoc code; Lomax et al. 2000). These authors follow the probabilistic formulation of inversion of Tarantola and Valette (1982) and Tarantola (1987). The grid of the probability density function (PDF) values obtained by the grid search represents the complete probabilistic spatial solution of the earthquake location problem. The maximum-likelihood (or minimum-misfit) point of the complete, non-linear location PDF is selected as an “optimal” hypocenter. To make the location program efficient for complex 3D models, the travel times between each station and all of the nodes of an x, y, z spatial grid were computed using a 3D version of the Eikonal finite differences scheme of Podvin and Lecomte (1991). To compute the travel times, a regular-sized spatial grid of $0.5 \times 0.5 \times 0.5 \text{ km}^3$ was used.

Figure 2 shows a map of the earthquake locations using the NonLinLoc algorithm and the 3D P-wave velocity model. The average values of location parameters are $\text{RMS} = 0.4 \text{ s}$, $\text{ERH} = 3.1 \text{ km}$, and $\text{ERZ} = 4.3 \text{ km}$. The aftershocks are located along the three fault segments that were associated with the mainshock of the 1980 Irpinia earthquake. Most of the earthquakes occurred within the first 20 km (upper crust).

The earthquake locations using the 3D velocity model do not show significant differences when compared with the locations obtained using the

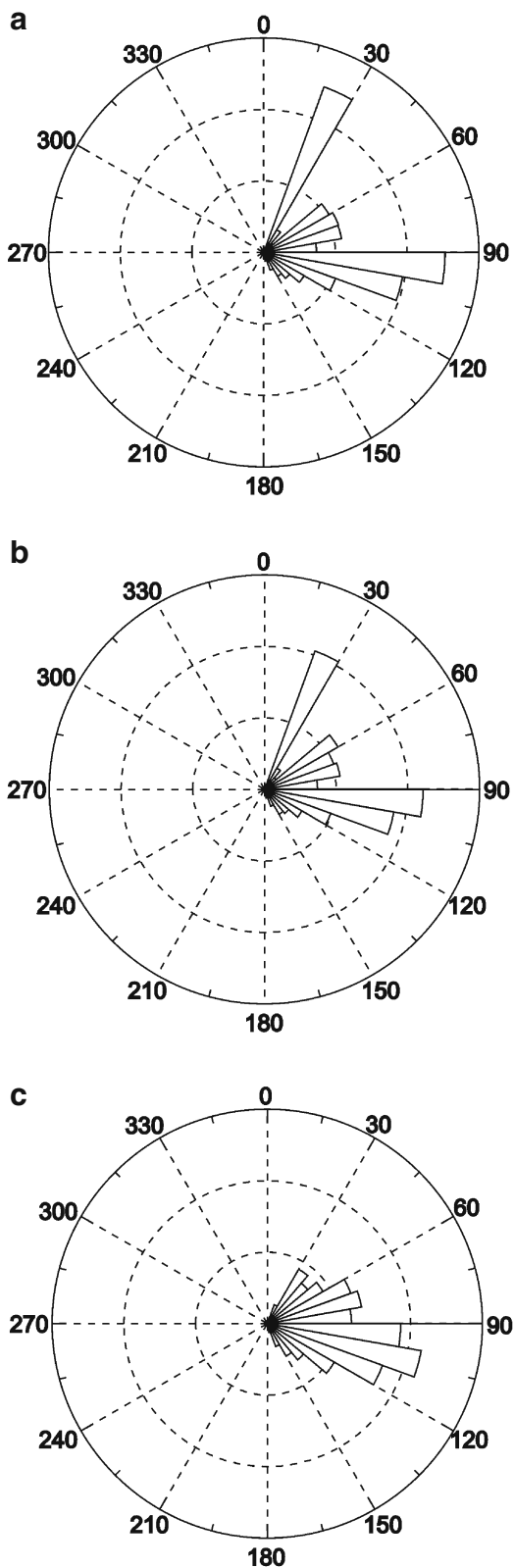
Fig. 2 Map of the Irpinia area showing: **a** aftershock epicenters (*circles*) and distribution of the stations of the INGV seismic network and the temporary mobile seismic network (*triangles*). A surface projection of the three fault segments (*thick black lines*) that ruptured during the 23 November 1980 Irpinia earthquake is also shown (from Pantosti and Valensise 1990). **b** E–W vertical section showing the hypocenter distribution of the aftershocks



Bernard and Zollo (1989) 1D layered velocity model although the earthquake location parameters (rms, erh, erz, gap) are slightly improved.

However, the basic difference lies in the computation of take-off angles. Rose diagram in Fig. 3a shows that the take-off angles computed using the 1D layered P-wave velocity model are centered around 30° and 90°. This is related to the

influence of the layers that make up the velocity model. As for the 1D layered velocity model, also the take-off angles computed using a 1D smooth velocity model ($v(z) = (2.27 + 0.4z)$ km/s) are centered mainly around 30° and 90° (Fig. 3b). The take-off angles, computed using the 3D velocity model, are more uniformly distributed (Fig. 3c).



◀ **Fig. 3** Rose diagram for the take-off angles computed using the **a** 1D layered, **b** 1D smooth, and **c** 3D P-wave velocity models. The length of the radius represents the 20% of data

4 The focal mechanisms

We estimated the focal mechanisms for the aftershocks of the 1980 Irpinia earthquake from the P-wave first-motion polarities using the FPFIT algorithm (Reasenberg and Oppenheimer 1985). FPFIT is a grid search routine that searches for the double-couple fault plane solution that provides the best fit of a given set of first-motion polarities observed for an earthquake.

To compute the high-quality focal mechanisms for the selected dataset of the Irpinia earthquakes, we decided to reject the earthquakes, located in the 3D velocity model, with less than six polarity readings, with horizontal (ERH) and vertical (ERZ) location errors larger than 0.8 km, with an RMS larger than 0.5 s, and with azimuthal gaps larger than 200°. Worthy of note is that we have considered only the P polarities relative to the P wave arrival time readings with the smaller reading error. This selection reduced the dataset from 2,352 to 321 earthquakes. Moreover, from the computed focal mechanisms, we have selected those mechanisms that had a single solution or at most only one discrepant polarity. For these, among the multiple fault plane solutions relative to the same earthquake, we have selected the focal mechanism which is more consistent with the focal mechanism of the 1980 Irpinia earthquake. In Fig. 4, examples of the quality of the fault plane solutions are shown. The final dataset consists of 139 focal mechanisms (see Table 1 and Fig. 5a).

Mostly, fault plane solutions belong to normal component faulting (pure normal fault and normal fault with a strike-slip component). Only some solutions show strike-slip or reverse faulting. For clearness, the horizontal projections of the extensional (T) axis are shown in Fig. 5b. The length of the small line is inversely proportional to the plunge of the T axis: longer lines represent T axes with smaller values of plunge. A more detailed analysis of these values displayed that

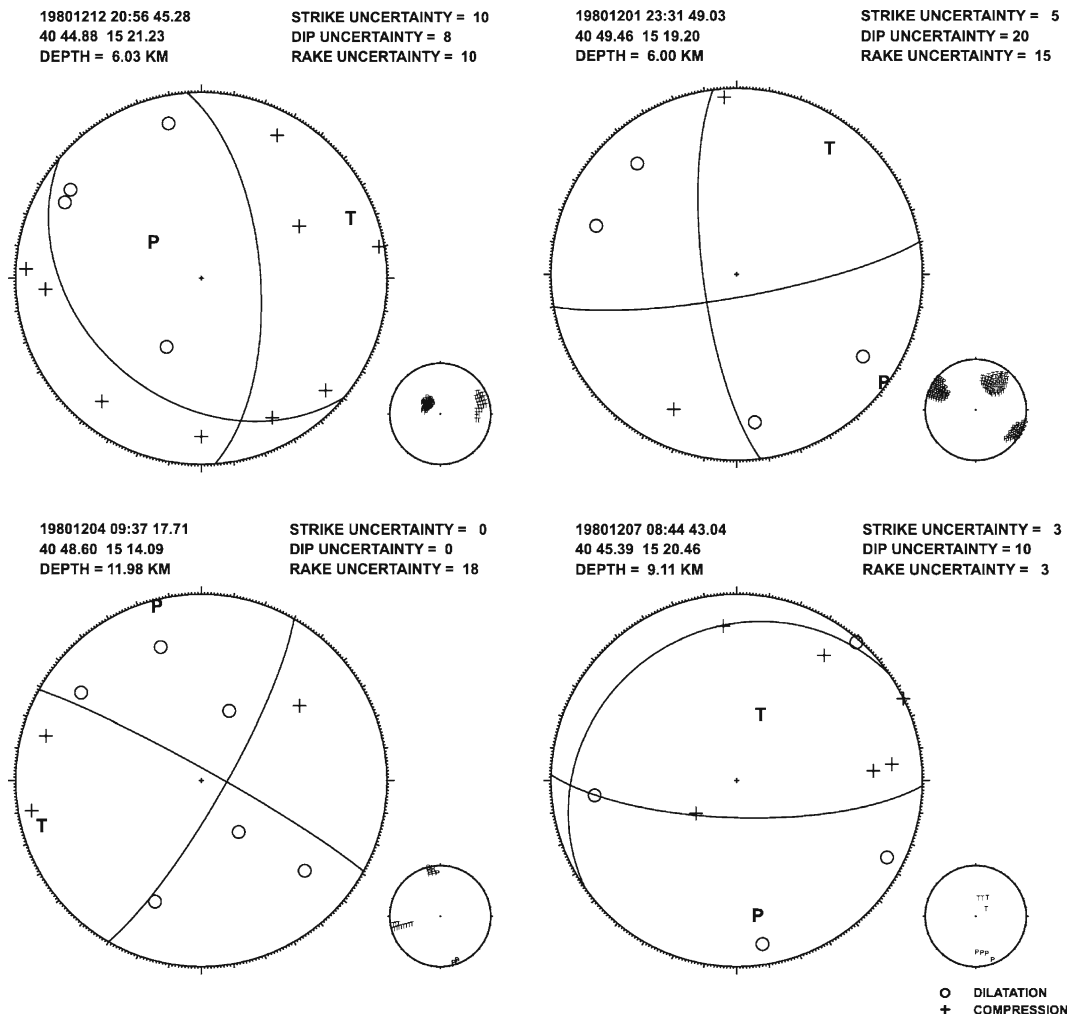


Fig. 4 Examples of the quality of the fault plane solutions

115 out of the 139 focal mechanisms have plunge of the *T* axis of less than 35° (Fig. 6a). The *T* axes show a predominant NE–SW direction. The *T* axes direction variability is shown in the rose diagram of Fig. 6b.

5 Stress inversion using events located in 1D and 3D velocity models

Generally the *P* axis and *T* axis of a single fault plane solution do not coincide with the maximum and minimum compressive stress orientations acting in the area (McKenzie 1969). Small

pre-existing faults in the shallow crust may be conducive to slip when only a small component of shear stress is resolved along the fault surface. For this reason, the earthquake focal mechanisms provide a source of data for stress determination (Michael 1987a). In this work, we used the method devised by Michael (1987a) to determine the stress field from a set of focal mechanisms. Many studies have developed several inverse techniques for finding the stress field orientation using slickenside data (fault orientation and slip direction). All of these methods are based on two assumptions: first, that the tangential traction on the fault plane should be parallel to the slip direction; and second, that the stress field is uniform within the

Table 1 Parameters of the 139 selected fault plane solutions

Date	T.O. (h/m/s)	Strike	Dip	Rake	
19801201	02/02/30.45	255	50	-60	f
19801201	05/49/4.26	310	30	55	f
19801201	23/31/49.03	170	80	165	a
19801202	04/11/19.68	20	25	-90	f
19801202	05/16/47.92	215	25	-85	a
19801202	08/28/32.41	0	40	-110	f
19801202	21/29/24.36	30	40	-60	f
19801204	00/41/29.15	30	40	-60	f
19801204	02/51/31.78	290	50	-5	a
19801204	06/14/45.35	180	60	-130	a
19801204	07/12/20.26	290	30	-20	f
19801204	09/37/17.71	120	80	5	f
19801204	16/22/5.05	50	75	-100	a
19801204	18/19/43.47	100	15	85	f
19801204	20/11/38.28	135	50	55	a
19801205	02/09/29.51	30	80	-150	a
19801205	02/38/31.33	280	75	-50	f
19801205	03/40/12.58	225	20	150	f
19801205	07/42/31.06	260	80	-105	f
19801206	02/00/12.3	195	65	-140	a
19801207	08/44/43.04	325	20	55	f
19801207	10/08/50.64	255	15	-65	f
19801207	13/30/5.16	85	70	-65	f
19801208	04/43/48.78	125	80	-70	f
19801208	16/06/34.92	335	15	-65	a
19801208	19/08/46.84	180	55	-90	a
19801208	20/08/29.26	0	20	-140	f
19801208	21/21/8.25	320	55	-15	a
19801208	23/09/58.14	340	60	-160	f
19801209	02/04/9.51	0	80	-110	a
19801209	02/31/9.87	95	75	-50	f
19801209	05/40/33.41	195	35	-175	a
19801209	09/05/35.2	295	65	20	f
19801209	14/27/25.52	310	15	-140	a
19801209	15/22/6.26	85	55	-100	a
19801209	15/24/29.69	200	50	70	f
19801209	16/28/4.14	280	30	25	f
19801209	19/19/4.61	235	15	-115	f
19801209	23/42/2.82	105	30	5	f
19801210	01/41/44.28	195	35	20	f
19801210	02/16/5.94	20	75	-105	a
19801210	04/50/54.44	230	25	-140	a
19801210	04/53/14.37	290	45	150	a
19801210	04/53/58.85	200	70	-75	a
19801210	07/55/34.51	120	80	20	f
19801210	12/41/26.56	90	30	-50	f
19801210	12/57/15	170	40	-110	a
19801210	14/08/14.38	340	20	180	a
19801210	14/42/31.3	100	55	-145	a
19801210	15/34/24.04	190	40	-140	f
19801210	16/55/32.78	255	20	-120	a
19801210	17/19/28.64	310	65	25	f
19801210	19/55/33.79	60	50	-5	a
19801210	21/18/36.27	15	80	165	a

Table 1 (continued)

Date	T.O. (h/m/s)	Strike	Dip	Rake	
19801210	21/20/29.16	65	80	-85	a
19801210	21/44/33.61	0	60	-70	a
19801210	22/14/6.82	30	65	-150	a
19801210	22/25/31.45	180	65	-110	a
19801211	01/42/24.02	285	45	-35	f
19801211	03/40/42.84	15	40	-55	a
19801211	06/00/12.38	25	35	-30	a
19801211	08/22/47.33	180	45	-85	a
19801211	09/31/6.94	240	20	-110	f
19801211	09/56/49.83	260	55	-140	f
19801211	10/40/10.65	50	40	-100	f
19801211	10/57/30.13	230	35	-65	a
19801211	12/25/19.45	120	5	-180	f
19801211	15/46/50.93	170	35	-160	f
19801211	15/52/3.97	285	30	170	a
19801211	16/32/14.63	10	40	-90	f
19801211	16/58/32.83	35	40	-105	a
19801211	17/10/19.08	25	40	-110	a
19801211	17/38/21.57	125	35	100	f
19801211	20/32/20.8	280	40	80	f
19801211	22/35/1.77	120	20	-40	a
19801211	23/28/25.23	175	35	-145	a
19801211	23/58/10.25	200	40	-90	a
19801212	00/59/12.41	160	20	-95	f
19801212	03/14/51.42	45	75	-20	a
19801212	08/20/56.78	285	75	-40	f
19801212	09/43/11.45	220	80	-105	f
19801212	10/49/12.39	25	15	40	a
19801212	11/43/42.45	275	25	-45	f
19801212	11/45/38.78	230	50	165	f
19801212	14/04/0.24	35	75	-15	a
19801212	14/14/46.55	350	25	-155	f
19801212	18/13/45.53	40	40	-80	f
19801212	18/29/9.66	350	75	-80	a
19801212	18/35/7.48	245	65	30	a
19801212	19/37/28.29	330	20	80	a
19801212	20/42/53.68	225	20	-115	f
19801212	20/56/45.28	220	35	-130	a
19801212	21/02/5.34	245	60	-85	a
19801212	21/38/2.28	45	75	15	f
19801212	22/05/19.57	5	35	-155	f
19801212	22/29/21.67	230	55	-55	a
19801213	00/12/50.78	160	80	135	f
19801213	00/49/47.51	175	20	-85	f
19801213	01/18/41.34	80	35	-60	f
19801213	02/32/6.11	200	15	-90	f
19801213	03/25/19.36	225	55	-65	a
19801213	03/28/1.86	225	70	-30	a
19801213	03/52/39.7	195	45	-120	a
19801213	10/24/7.68	95	30	-40	f
19801213	14/32/22.89	275	25	-25	a
19801213	14/41/25.18	190	5	-100	f
19801213	16/42/49.03	215	35	-105	f
19801213	18/11/20.33	210	25	-95	a

Table 1 (continued)

Date	T.O. (h/m/s)	Strike	Dip	Rake	
19801213	21/43/34.95	220	60	−100	f
19801213	22/29/23.54	265	55	−80	a
19801213	23/03/41.61	55	40	−90	f
19801214	01/07/14.58	340	30	−80	f
19801214	02/30/23.04	205	20	−80	f
19801214	03/47/19.65	20	25	−35	f
19801214	06/07/47.6	305	30	0	a
19801214	07/15/56.36	90	70	−65	f
19801214	11/24/30.9	60	45	−100	f
19801214	16/34/10.72	15	45	−90	f
19801214	16/39/44.9	70	45	−100	f
19801214	17/07/37.71	220	30	−140	a
19801214	17/47/45.43	230	35	−155	a
19801214	18/18/50.76	200	80	−125	a
19801214	19/13/14.8	200	80	120	a
19801214	19/13/44.09	0	40	−25	f
19801214	22/24/42.1	240	40	−175	f
19801214	23/48/22.94	0	35	−125	f
19801215	00/10/23.53	285	25	−95	a
19801215	00/21/5.48	170	60	−55	f
19801215	00/24/31.86	10	55	−140	a
19801215	00/55/40.38	255	80	−30	a
19801215	01/54/59.9	205	40	−155	a
19801215	04/00/9.05	250	45	−165	f
19801215	04/45/2.36	0	60	−145	a
19801215	05/21/46.86	65	35	−80	f
19801215	05/26/26.41	100	35	15	f
19801215	06/42/55.91	30	40	−105	a
19801215	12/11/23.88	300	70	15	f
19801215	19/52/5.9	100	45	−65	f
19810115	11/12/42.6	265	60	−65	a

The letters f and a denote the fault and auxiliary planes respectively, determined after the stress inversion

studied area (Gephart and Forsyth 1984; Michael 1984; Angelier 1990). The use of fault plane solutions is a much more difficult problem with respect to slickenside data because of the fault/auxiliary plane ambiguity. The best algorithm would use a set of fault plane solutions as input and would give the correct choices of fault planes and the best-fit stress tensor as output. Ellsworth and Zhonghuai (1980) suggested that every possible set of fault plane choices should be considered and inverted. The set of fault planes and slip vectors that fits a single best stress tensor contains the correct choices, and the stress tensor they inferred is the correct stress tensor. This problem was worked out by Gephart and Forsyth (1984) following a grid search methodology. The algorithm developed by Michael (1987a) is based on that formulation. Applying the Michael technique to a set

of focal mechanisms, we obtain the best stress tensor that fits the data and is represented by the orientation of the three principal stress axes, and the scalar which describes the relative magnitudes of the principal stresses and hence constrains the shape of the deviatoric stress ellipsoid, known as parameter ϕ . This parameter is expressed as:

$$\phi = \frac{\sigma_2 - \sigma_3}{\sigma_1 - \sigma_3}$$

where σ_1 , σ_2 , and σ_3 are the maximum, the intermediate, and the minimum compressive principal stress axis, respectively.

The basic characteristic of the Michael (1987a) algorithm is the computation of the confidence limits of the principal stress axes directions. Confidence limits are computed by a statistical tool known as bootstrap resampling. From a theoret-

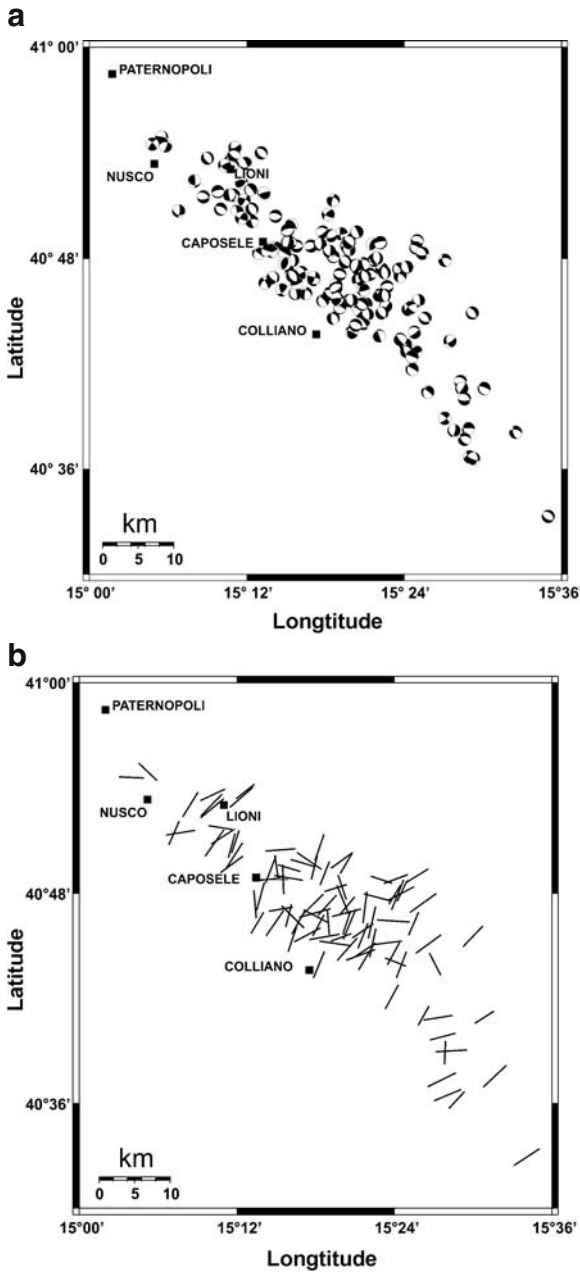


Fig. 5 **a** Map showing the distribution of the 139 selected focal mechanisms from the 1980 earthquake epicenter region computed using the P-wave polarity data. The parameters of the computed fault plane solutions are given in Table 1. **b** Distribution of the focal mechanism *T* axes. The lengths of the bars are inversely proportional to the plunge of the *T* axes

ical point of view, confidence limits would be computed by repeating the full experiment many times. To simulate a repetition of the experiment,

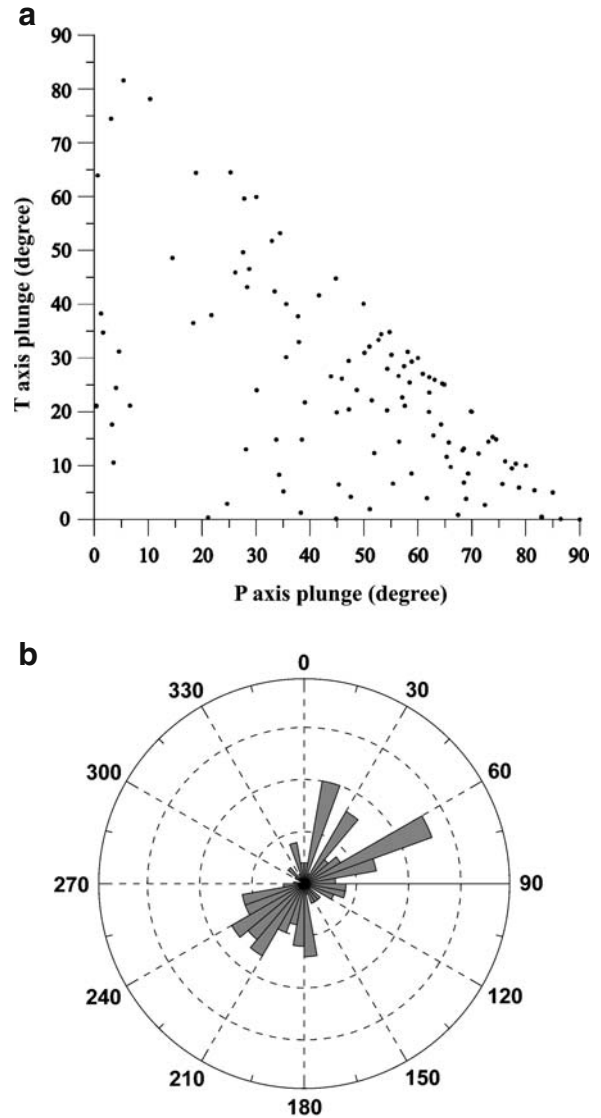


Fig. 6 **a** Plunge of *T* and *P* axis diagram. **b** Rose diagram for the focal mechanism *T* axes (the length of the radius represents the 15% of data)

we pick data (focal mechanisms) at random from the original dataset. This new dataset will have the same number of data as the original dataset, but will have same mechanisms repeated two or more times while other mechanisms will be absent (Michael 1987a). We inverted this dataset for the stress field, and repeated this process 2,000 times. For example, to define the 95% confidence region, we generated 2,000 new datasets to provide new stress tensors, and the 95% confidence region is

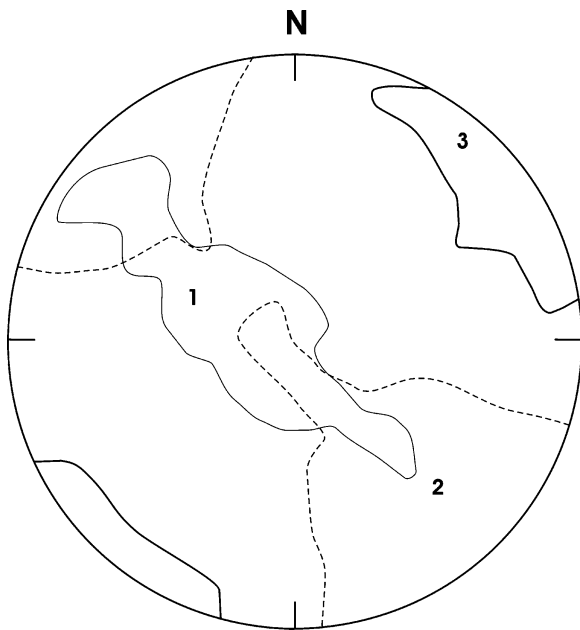


Fig. 7 Stereonet plot with the results of the stress inversion using focal mechanism data. The numbers 1, 2, and 3 are the projection of the principal stress axes: σ_1 , σ_2 , and σ_3 , respectively. The *thin, dashed, and thick lines* circumscribe the 95% confidence regions for σ_1 , σ_2 , and σ_3 , respectively

defined by the 95% stress tensors that had the highest normalized scalar product, with the stress tensor determined by the original dataset. The normalized scalar product is a measure of the closeness between two tensors and it is defined as:

$$\frac{\sum_{i=1}^3 \sum_{j=1}^3 B_{ij} C_{ij}}{\left(\sum_{i=1}^3 \sum_{j=1}^3 B_{ij}^2 \right)^{1/2} \left(\sum_{i=1}^3 \sum_{j=1}^3 C_{ij}^2 \right)^{1/2}}$$

where B and C are two tensors.

Empirical tests showed that 2,000 repetitions are enough to yield a stable result (Michael 1987b).

6 Results

To estimate the stress field in the present study, we analyzed the focal mechanisms of low magnitude earthquakes. Since we cannot decide *a priori* which nodal plane is the fault plane, we used

the Michael (1987a) algorithm, which uses both nodal planes to attempt to choose the correct fault planes while determining the best stress tensor. We also estimated the error on the principal stress axes direction by computing the 95% confidence regions through resampling the data 2,000 times with the bootstrap procedure.

Figure 7 shows a typical representation of the inversion results: the principal stress axes (σ_1 , σ_2 , σ_3) with their confidence regions are plotted into the lower hemisphere stereonet. The results obtained by inverting all of the selected focal mechanisms show a nearly horizontal NE–SW minimum compressive stress axis (σ_3) and a maximum compressive stress axis (σ_1) that is nearly vertical. Although axis σ_3 is horizontal, with a small error on its dip, there is a large uncertainty for its trend, while axis σ_1 shows a large error both for trend and plunge.

To understand if the reason of these large confidence regions is due to the use of a heterogeneous dataset, we used the multi-inverse method proposed by Yamaji (2000), which is a numerical technique that is used to separate stresses from heterogeneous fault-slip data. In this way, if our dataset consists of more sets of homogeneous data, the Yamaji method allows us to identify the stress fields compatible with the various subsets. The results are shown in Fig. 8, where the directions of the σ_1 and σ_3 axes are indicated by dots on the lower hemisphere equal-area net to the left and right, respectively. On the left of Fig. 8, the direction of the bars extending from the dots indicates the azimuth of the corresponding σ_3 direction, while its lengths indicate the plunge of the σ_3 axis. In the right panel, the roles of the bars and dots are assigned inversely: the lengths and directions of the bars indicate the σ_1 plunge and azimuth, respectively. Each symbol represents a state of stress and its color represents a stress ratio value (ϕ). Where the dataset includes two stresses that are compatible with two sets of data, the results show two clusters representing the two stresses. The clusters of dot-bar symbols with the same color and the same bar direction represent significant stresses. In Fig. 8, which was obtained using the selected dataset, the results show a single solution with a large uncertainty,

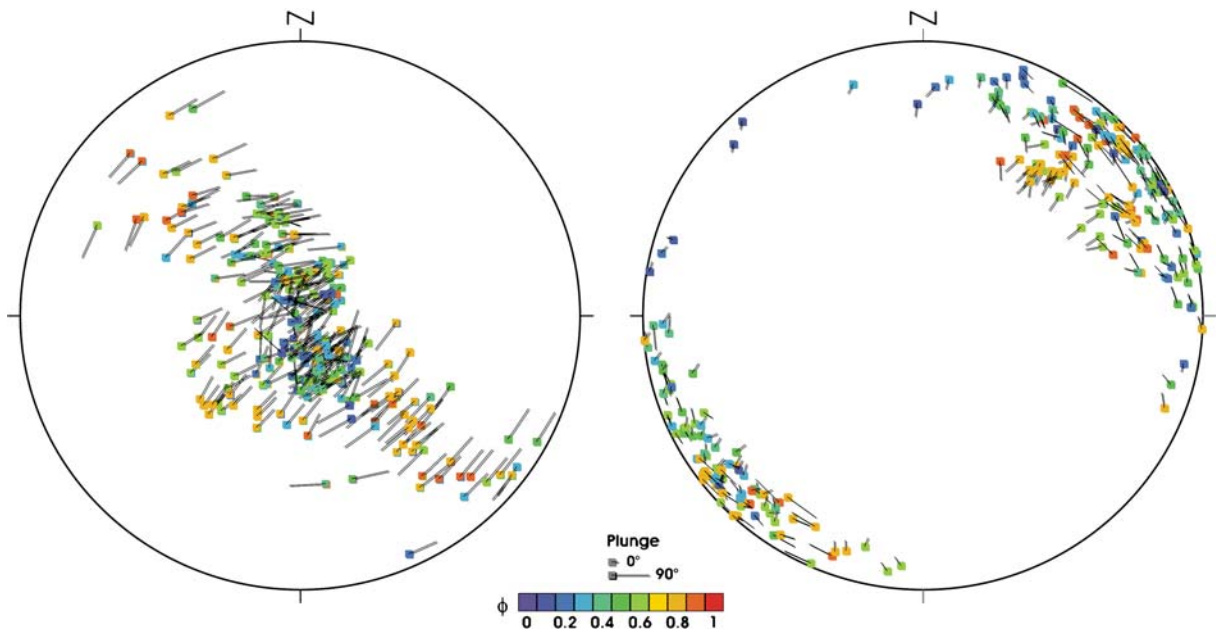


Fig. 8 The result of the multi-inverse method (Yamaji 2000) applied to the data. Each *symbol* represents a state of stress; the stress ratio is represented by the *color*, and the direction of the stress axes is indicated by the position and direction of the *symbol*. The directions of the σ_1 and σ_3 axes are indicated by *dots* on the lower hemisphere equal-

area projections on the left and the right, respectively. In the *left panel*, the directions of the *bars* extending from the *dots* indicate the azimuth of the corresponding σ_3 direction. The lengths of the *bars* indicate the σ_3 plunge. On the *right panel*, the roles of the *bars* and *dots* are assigned inversely. The lengths of the *bars* indicate the σ_1 plunge

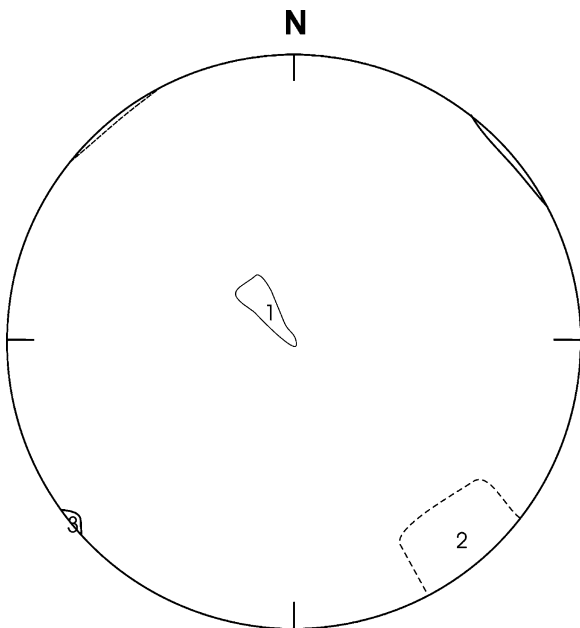


Fig. 9 Stress inversion result using the 115 focal mechanisms with T axis plunge $\leq 35^\circ$

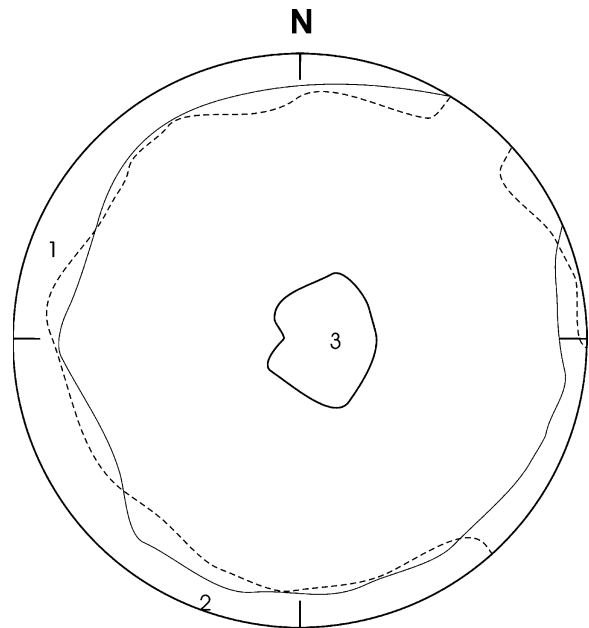


Fig. 10 Stress inversion result using the 24 focal mechanisms with T axis plunge $> 35^\circ$

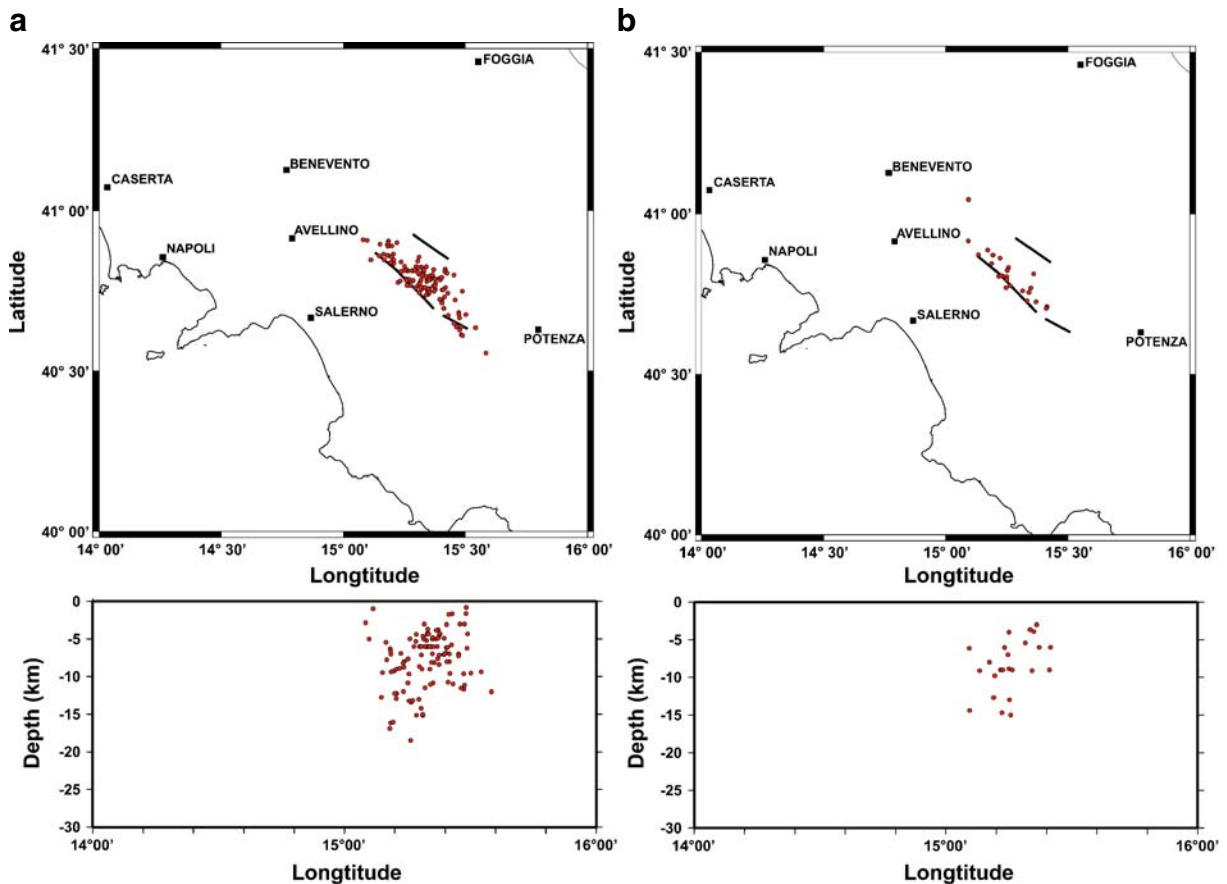


Fig. 11 Earthquake hypocentral location of events with focal mechanisms with T axis plunge **a** $\leq 35^\circ$ and **b** $> 35^\circ$

similar to results obtained using the Michael algorithm.

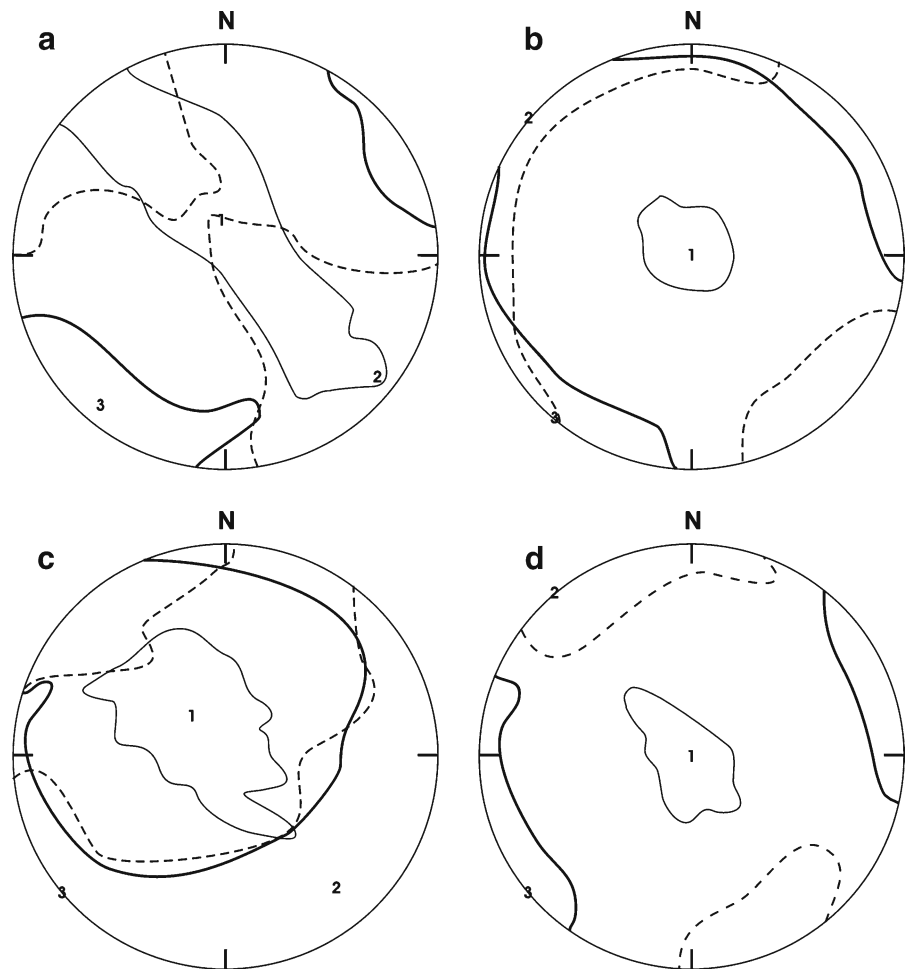
These results show that the dataset is homogeneous and there are no subsets of data that could be the cause of the uncertainty associated with the principal axis directions. We only inverted 115 of the 139 focal mechanisms that show a plunge of the T axis less than 35° to determine the best stress tensor and we obtain the results shown in Fig. 9. The obtained stress field shows a NE–SW extension, with a horizontal σ_3 (plunge 0° , trend 230°) and a vertical σ_1 (plunge 80° , trend 320°). This stress tensor orientation shows small confidence regions of the principal stresses axes and is consistent with the previous solution obtained using all of the data (see Fig. 7).

These results also show that the large confidence regions of the principal stresses axes, computed using the complete dataset (Fig. 7), are

caused only by few data, those with T axis plunge larger than 35° (24 focal mechanisms). Moreover, the inversion of this small dataset shows an undetermined solution, mainly for the σ_1 and σ_2 axes (Fig. 10). Worthy of note is that the σ_3 axis confidence region is completely not overlapping with that obtained by inverting all the dataset (Fig. 7). This means that the inversion result obtained by inverting only the 24 focal mechanisms is greatly not consistent with that obtained using the complete dataset.

Considering the consistence between the stress field obtained with all of the data and that obtained by inverting the focal mechanisms with a plunge of the T axis $\leq 35^\circ$, which represent 83% of the complete focal mechanisms, we ascribe the remaining mechanisms to local heterogeneities of the stress field. Figure 11a and b show hypocentral location of earthquakes belonging to both

Fig. 12 Stress field results from focal mechanisms of selected earthquakes located in 1D smooth (a) and layered (c) P-wave velocity models. b stress inversion result using the focal mechanisms with T axis plunge $\leq 35^\circ$ for 1D smooth and 1D layered models (d). See Fig. 7 for a description of this figure



the two subsets characterized by different T axes plunge ($T \leq 35^\circ$ and $T > 35^\circ$): the earthquake locations do not show a meaningful hypocentral splitting between the two subsets with focal mechanisms. The stress inversion results obtained with the inversion of the 115 focal solutions suggest a N 50° E-oriented minimum principal stress σ_3 , and reveals that the epicenter region of the 1980 earthquake is ongoing through a NE–SW extension.

In order to verify if the results obtained using the 3D velocity model are better constrained compared to the results based on 1D velocity models, we have repeated the stress inversion using 1D layered and smooth velocity models. As for the selected earthquakes located in the 3D P waves velocity model, also for events located in the 1D velocity models (layered and smooth), we have computed the focal mechanisms and inverted the

selected subsets for stress field inversion. In particular, the results of focal mechanisms inversion of earthquakes located in the 1D smooth velocity model show large uncertainty for orientations of principal stress axes (Fig. 12a) in respect to the results obtained using the earthquakes located in the 3D model. Also, the results obtained using focal mechanisms with plunge of the T axis less than 35° show large confidence regions, mainly for σ_2 and σ_3 , while σ_1 is better constrained (Fig. 12b). Similar results have been obtained using the 1D layered P waves velocity model (Fig. 12c and d).

The results obtained in this work are compared with those obtained by the use of different methodologies applied recently in Southern Apennines studies and summarized in Fig. 13. In particular, Amato and Montone (1997) and Montone et al. (1999) studied the active stress in

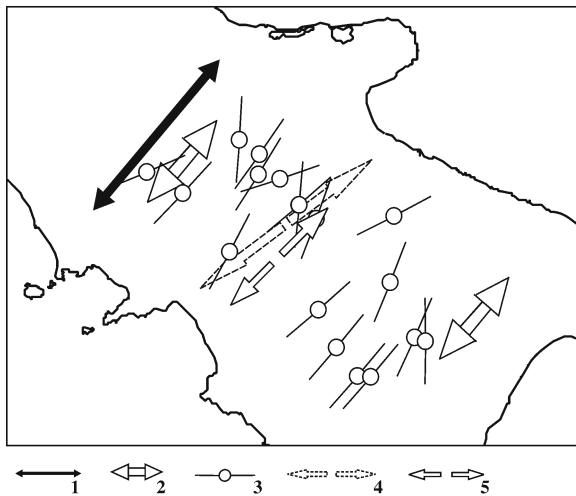


Fig. 13 Stress field orientations obtained from former studies using: 1 GPS data (Anzidei et al. 2001); 2 strong earthquakes (Montone et al. 1999); 3 breakout data (Montone et al. 1999); 4 focal mechanisms of the Southern Apennines earthquakes Frepoli and Amato (2000); 5 this study

the Southern Apennines through the analysis of breakout and fault plane solution data of moderate to strong earthquakes. They inferred that the Southern Apennines is ongoing through a NE–SW extension, with a horizontal σ_3 and a vertical σ_1 . Frepoli and Amato (2000) used focal mechanisms of the Southern Apennines earthquakes that occurred in the last 20 years to obtain information about the stress field. The inversion of these fault plane solutions, which were mainly normal faults, showed an extensional stress field along a NE–SW direction. Analysis of GPS data also provides a significant SW–NE extension in the Southern Apennines (Anzidei et al. 2001).

7 Conclusions

Focal mechanisms of earthquakes from the Irpinia Region have been used to determine the average stress field acting in the area. The dataset is given by aftershocks that follow the 23 November 1980 Irpinia earthquake (M 6.9).

The availability of a 3D velocity model (Romeo et al. 2007) allowed us to relocate the earthquakes using a non-linear probabilistic global search algorithm (NonLinLoc—Lomax et al. 2000) to obtain

an accurate hypocentral location especially for the finding out the take-off angle values, a basic parameter in the focal mechanisms computation. As a matter of fact, the take-off angles computed using the 3D P-wave velocity model show within a rose diagram a more uniform distribution with respect to those computed using 1D velocity models.

Although the original dataset is large (2,352 earthquakes), our restrictions on the location parameters and the quality of the focal mechanism considerably decreased the amount of data used in this study. Usually, the use of fault plane solutions to determine the stress field shows two different problems: (1) low magnitude earthquakes can be associated with local stress field heterogeneity within a studied area; and (2) the focal mechanism data is characterized by the ambiguity between the fault and the auxiliary planes.

We used the algorithm developed by Michael (1987a), which attempts to choose the correct fault plane while determining the stress tensor, following the assumption that all of the data are consistent with a uniform stress field. The homogeneity of the data was verified using the multi-inverse method developed by Yamaji (2000). The large part (115 out of 139) of the focal mechanisms shows a T axis plunge $\leq 35^\circ$. The results of the inversion show that, using 115 of the 139 focal mechanisms, the best stress tensor obtained is characterized by a horizontal minimum compressive stress axis (σ_3) NE–SW oriented and a vertical maximum compressive stress axis (σ_1), with small (95%) confidence regions. The remaining data have been explained as focal mechanisms belonging to local heterogeneity of the stress field within the studied area. These data are not consistent with a well constrained stress field, and if they are included in the inversion they increase the uncertainty of the principal stress axes direction.

The comparison of stress tensors inverted on the basis of 1D and 3D velocity models shows that the 3D model represents the main progress providing the better constrained stress field.

The agreement between the results of this study and those obtained using strong to moderate earthquake focal mechanisms and breakout data reveals that low magnitude seismicity represents a useful tool for the determination of stress fields,

especially in regions where there is no evidence of surface faulting.

References

- Amanti M, Bontempo R, Cara P, Conte G, Di Bucci D, Lembo P, Pantaleone NA, Ventura R (2002) Carta Geologica d'Italia Interattiva. 1:100000, SGN, SSN, ANAS, 3 CD-ROM
- Amato A, Montone P (1997) Present-day stress field and active tectonics in southern peninsular Italy. *Geophys J Int* 130:519–534. doi:[10.1111/j.1365-246X.1997.tb05666.x](https://doi.org/10.1111/j.1365-246X.1997.tb05666.x)
- Amato A, Chiarabba C, Malagnini L, Selvaggi G (1992) Three-dimensional P-velocity structure in the region of the Ms = 6.9 Irpinia, Italy, normal faulting earthquake. *Phys Earth Planet Inter* 75:111–119. doi:[10.1016/0031-9201\(92\)90122-C](https://doi.org/10.1016/0031-9201(92)90122-C)
- Angelier J (1990) Inversion of field data in fault tectonics to obtain the regional stress—III. A new rapid direct inversion method by analytic means. *Geophys J Int* 103:363–376. doi:[10.1111/j.1365-246X.1990.tb01777.x](https://doi.org/10.1111/j.1365-246X.1990.tb01777.x)
- Anzidei M, Baldi P, Casula G, Galvani A, Mantovani E, Pesci A, et al. (2001) Insights into present-day crustal motion in the central Mediterranean area from GPS surveys. *Geophys J Int* 146:98–110. doi:[10.1046/j.0956-540x.2001.01425.x](https://doi.org/10.1046/j.0956-540x.2001.01425.x)
- Bernard P, Zollo A (1989) The Irpinia (Italy) 1980 earthquake: detailed analysis of a complex normal faulting. *J Geophys Res* 94:1631–1647. doi:[10.1029/JB094iB02p01631](https://doi.org/10.1029/JB094iB02p01631)
- Bott MHP (1959) The mechanisms of oblique slip faulting. *Geol Mag* 96:109–117
- D'Argenio B, Pescatore TS, Scandone P (1974) Schema geologico dell'Appennino Meridionale (Campania e Lucania). *Atti del Convegno: Moderne Vedute sulla Geologia dell'Appennino Meridionale*. Accad Naz Lincei (Rome) 183:49–72
- Del Pezzo E, Iannaccone G, Martini M, Scarpa R (1983) The 23 November 1980 southern Italy earthquake. *Bull Seismol Soc Am* 73:187–200
- Deschamps A, King GCP (1984) Aftershocks of the Campania–Lucania (Italy) earthquake of the 23 November 1980. *Bull Seismol Soc Am* 74:2483–2517
- Ellsworth WL, Zhonghuai X (1980) Determination of the stress tensor from focal mechanism data. *Eos Trans AGU* 61:1117 (abstract)
- Frepoli A, Amato A (2000) Spatial variation in stress in peninsular Italy and Sicily from background seismicity. *Tectonophysics* 317:109–124. doi:[10.1016/S0040-1951\(99\)00265-6](https://doi.org/10.1016/S0040-1951(99)00265-6)
- Gephart JW, Forsyth DW (1984) An improved method for determining the regional stress tensor using earthquake focal mechanism data: application to the San Fernando earthquake sequence. *J Geophys Res* 89:9305–9320. doi:[10.1029/JB089iB11p09305](https://doi.org/10.1029/JB089iB11p09305)
- Giardini A (1993) Teleseismic observation of the November 23 1980, Irpinia earthquake. *Ann Geofis* XXXVI:17–25.
- Improta L, Iannaccone G, Capuano P, Zollo A, Scandone P (2000) Inference on the upper crustal structure of the Southern Apennines (Italy) from seismic refraction investigations and subsurface data. *Tectonophysics* 317:273–297. doi:[10.1016/S0040-1951\(99\)00267-X](https://doi.org/10.1016/S0040-1951(99)00267-X)
- Improta L, Bonagura M, Capuano P, Iannaccone G (2003) An integrated geophysical investigation of the upper crust in the epicentral area of the 1980, M = 6.9, Irpinia earthquake (Southern Italy). *Tectonophysics* 361:139–169. doi:[10.1016/S0040-1951\(02\)00588-7](https://doi.org/10.1016/S0040-1951(02)00588-7)
- Lomax A, Virieux J, Volant P, Thierry BC (2000). Probabilistic earthquake location in 3D and layered models. Kluwer Academic, Dordrecht, pp 101–134
- McGarr A, Gay NC (1978) State of stress in the Earth's crust. *Annu Rev Earth Planet Sci* 6:405–436. doi:[10.1146/annurev.ea.06.050178.002201](https://doi.org/10.1146/annurev.ea.06.050178.002201)
- McKenzie DP (1969) The relation between fault plane solutions for earthquakes and the directions of the principal stresses. *Bull Seismol Soc Am* 59:591–601
- McKenzie DP (1972) Active tectonics of the Mediterranean region. *Geophys J R Astron Soc* 30:109–185
- Menardi A, Rea G (2000) Deep structure of the Campania–Lucania arc (Southern Apennines, Italy). *Tectonophysics* 324:239–265. doi:[10.1016/S0040-1951\(00\)00137-2](https://doi.org/10.1016/S0040-1951(00)00137-2)
- Michael AJ (1984) Determination of stress from slip data: faults and folds. *J Geophys Res* 89:11517–11526. doi:[10.1029/JB089iB13p11517](https://doi.org/10.1029/JB089iB13p11517)
- Michael AJ (1987a) Use of the mechanisms to determine stress: a control study. *J Geophys Res* 92:357–368. doi:[10.1029/JB092iB01p00357](https://doi.org/10.1029/JB092iB01p00357)
- Michael AJ (1987b) Stress rotation during the Coalinga aftershock sequence. *J Geophys Res* 92:7963–7979. doi:[10.1029/JB092iB08p07963](https://doi.org/10.1029/JB092iB08p07963)
- Montone P, Amato A, Pondrelli S (1999) Active stress map of Italy. *J Geophys Res* 104:25595–25610. doi:[10.1029/1999JB900181](https://doi.org/10.1029/1999JB900181)
- Pantosti D, Valensise G (1990) Faulting mechanism and complexity of the November 23, 1980, Campania–Lucania earthquake, inferred from surface observations. *J Geophys Res* 95:15319–15341. doi:[10.1029/JB095iB10p15319](https://doi.org/10.1029/JB095iB10p15319)
- Patacca E, Scandone P (1989) Post-Tortonian mountain building in the Apennines: the role of the passive sinking of a relic lithospheric slab. In: Boriani, Bonafede M, Piccadio GB, Vai eGB (eds) *The lithosphere in Italy*. *Acc Naz Lincei* 80:157–176
- Patacca E, Sartori R, Scandone P (1990) Tyrrhenian basin and Apenninic arc: kinematic relations since Late Tortonian times. *Mem Soc Geol Ital* 5:425–451
- Podvin P, Lecomte I (1991) Finite difference computation of traveltimes in very contrasted velocity models: a massively parallel approach and its associated tools. *Geophys J Int* 105:271–284. doi:[10.1111/j.1365-246X.1991.tb03461.x](https://doi.org/10.1111/j.1365-246X.1991.tb03461.x)
- Reasenberg P, Oppenheimer D (1985) Fpfit, Fpplot and Fppage. Fortran computer programs for calculating

- and displaying earthquake fault-plane solutions. U.S. Geol. Surv., Open-File Report 85–739
- Rivera L, Cisternas A (1990) Stress tensor and fault plane solution for a population of earthquakes. *Bull Seismol Soc Am* 80:600–614
- Romeo A, De Matteis R, Pasquale G, Iannaccone G, Zollo A (2007). Crustal structure and stress field for southern Apennines Region from local earthquakes. 24th International Union of Geodesy and Geophysics General Assembly, Perugia, Italy, July 2–13 2007
- Roure F, Casero P, Vially R (1991) Growth processes and melange formation in the Southern Apennines accretionary wedge. *Earth Planet Sci Lett* 102:395–412. doi:[10.1016/0012-821X\(91\)90031-C](https://doi.org/10.1016/0012-821X(91)90031-C)
- Tarantola A (1987) Inverse problem theory: methods for data fitting and model parameter estimation. Elsevier, Amsterdam
- Tarantola A, Valette B (1982) Inverse problems = quest for information. *J Geophys Res* 50:159–170
- Tiberti MM, Orlando L, Di Bucci D, Bernabini M, Parotto M (2005) Regional gravity anomaly map and crustal model of the Central-Southern Apennines (Italy). *J Geodyn* 40:73–91. doi:[10.1016/j.jog.2005.07.014](https://doi.org/10.1016/j.jog.2005.07.014)
- Westaway R, Jackson JA (1987) The earthquake of 1980 November 23 in Campania–Basilicata (Southern Italy). *Geophys J R Astron Soc* 90:375–443
- Yamaji A (2000) The multiple inverse method: a new technique to separate stresses from heterogeneous fault-slip data. *J Struct Geol* 22:441–452. doi:[10.1016/S0191-8141\(99\)00163-7](https://doi.org/10.1016/S0191-8141(99)00163-7)